arXiv:1704.04211v2 [cond-mat.mtrl-sci] 17 Apr 2017

Topologically Invariant Double Dirac States in Bismuth based Perovskites: Consequence of Ambivalent Charge States and Covalent Bonding

Bramhachari Khamari, Ravi Kashikar and B. R. K. Nanda*
Condensed Matter Theory and Computational Lab, Department of Physics, Indian Institute of Technology Madras, Chennai, India, 600036
(Dated: April 18, 2017)

Bulk and surface electronic structures, calculated using density functional theory and a tight-binding model Hamiltonian, reveal the existence of two topologically invariant (TI) surface states in the family of cubic Bi perovskites ($ABiO_3$; A = Na, K, Rb, Cs, Mg, Ca, Sr and Ba). The two TI states, one lying in the valence band (TI-V) and other lying in the conduction band (TI-C) are formed out of bonding and antibonding states of the Bi-{s,p} - O-{p} coordinated covalent interaction. Below a certain critical thickness of the film, which varies with A, TI states of top and bottom surfaces couple to destroy the Dirac type linear dispersion and consequently to open surface energy gaps. The origin of s-p band inversion, necessary to form a TI state, classifies the family of $ABiO_3$ into two. For class-I (A = Na, K, Rb, Cs and Mg) the band inversion, leading to TI-C state, is induced by spin-orbit coupling of the Bi-p states and for class-II (A = Ca, Sr and Ba) the band inversion is induced through weak but sensitive second neighbor Bi-Bi interactions.

I. INTRODUCTION

Topological insulators, which are insulating in bulk but with a invariant conducting surface/edge state in films [1–13], have gained considerable attention in the last decade. As it is a band phenomena arising out of the interplay between crystal and orbital symmetries, there have been extensive studies on the band structures of a large number of prototypes which include Bi based selenides and tellurides [14], open structures like skutterudites [15], Heusler compounds [16] and Bi based perovskites ($ABiO_3$) - 'A' being an alakali or alkaline earth metal[17–19]. The family of perovskites are very distinct from the rest. Firstly, here the topologically invariant (TI) surface states appear when Bi forms the octahedral complex with oxygen. Therefore, transition metal oxides like $BiFeO_3$, where the transition metals form the octahedral complex, are ruled out while the low temperature superconducting materials like $KBiO_3$ and $BaBiO_3$ are actively investigated. Secondly, unlike the other topological insulators, in $ABiO_3$ the TI state does not appear at the Fermi level (E_F) and instead, it appears far away from the Fermi level (E_F) in the conduction band [17].

There are a number of significant issues that remain unanswered on the formation of TI states in the family of Bi based perovskites. The cause of formation of a TI state in the conduction band, rather than on the E_F has not been explained. While most of the experimental and theoretical investigations are restricted to $KBiO_3$ and $BaBiO_3$, there are many other alkali (Na, Rb and Cs) and alkaline (Mg, Ca and Sr) elements which are expected to form the perovskite crystal structure of $ABiO_3$. Hence a thorough investigation of these compounds will shed light on the underlying physics of the formation of TI states in this family. While in the context of $BaBiO_3$ the TI state in the conduction band has been reported and analyzed [17], a recent study on $KBiO_3$ suggests that there are two TI states, approximately 9 eV apart with one in the conduction band and other in the valence band [18]. It has not been understood and substantiated whether the formation of "two TI states" is a characteristic feature of this family.

In the Bi based TI compounds like tellurides and selenides [14] the band inversion, which is a necessary criteria to form TI surface states, has been found to be an outcome of either strong spin-orbit coupling (SOC) of the Bi-p states or strain effect [4, 10, 20, 21]. In the case of perovskites, while in $KBiO_3$ SOC creates the band inversion[18], in $BaBiO_3$ the band inversion is present even in the absence of SOC [17]. A very recent study on Bi based double perovskites A_2BiXO_6, where A is a divalent cation like Ca, Sr and Ba, and X is either Br and I, also suggests that the band inversion is not led by SOC [22]. Since BiO_6 octahedra is a common feature in the crystal structure of these single and double perovskites, it is imperative to devise the mechanism of band inversion in the family of perovskites and classify the systems accordingly. The surface electronic structure so far have been examined using minimal basis set based tight binding (TB) Hamiltonian instead of a full basis set based first principles calculations [17–19]. In such studies, while the surface confinement effects are well taken into account, the microscopic changes in the chemical bonding, which affect the surface states significantly, are often ignored.

In this paper, we have examined the band structures of cubic perovskite $ABiO_3$, where A is either a monovalent cation (Na, K, Rb, Cs) or a divalent cation (Mg, Ca, Sr and Ba). The band structures are obtained from both density functional theory (DFT) and TB calculations. The former is achieved within the framework of full potential and plane wave basis set based FP-LAPW method [23]. The TB Hamiltonian is formulated based on Linear Combination of Atomic orbitals (LCAO) method as

* nandab@iitm.ac.in

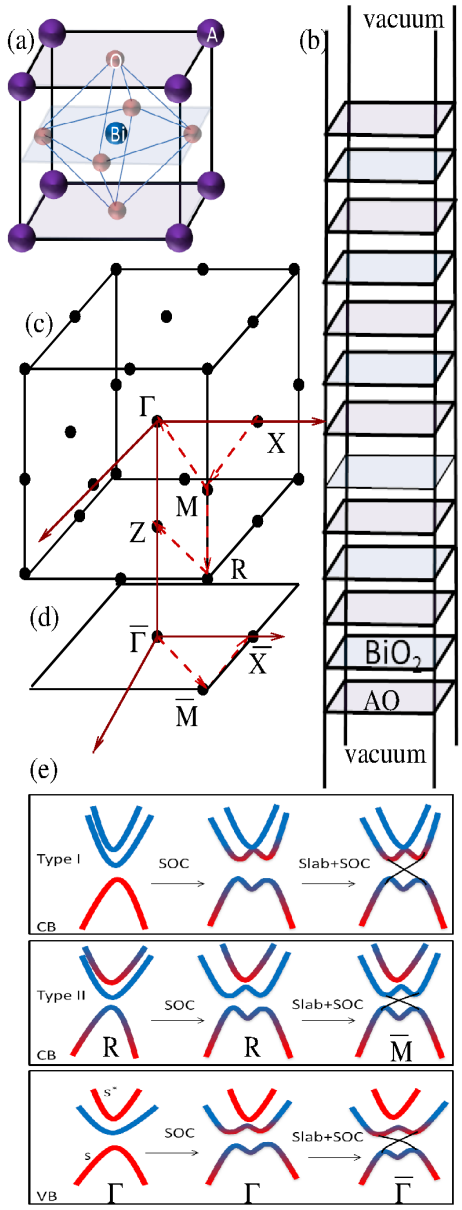

FIG. 1. (a) Crystal structure of cubic perovskite $ABiO_3$ with the illustration of BiO_6 octahedra. The crystal can also be considered as consisting of AO and BiO_2 planes stacked alternately along the 001 direction. (b) The $ABiO_3$ slab grown along 001. (c and d) The bulk and surface Brillouin zone with high symmetry points. (e) Schematic illustration of mechanism of band inversion and formation of topologically invariant surface states.

developed by Slater and Koster [24]. Fig. 1 summarizes the important findings in this work. Two TI states, one in valence band and other in conduction band are characteristic features of Bi based perovskites. While the TI state in the valence band (TI-V) is formed by the bonding states, resulted from O-$\{p\}$ - Bi-$\{s, p\}$ strong covalent hybridization, the TI state in the conduction band (TI-C) is formed by the corresponding anti-bonding states. The band inversion for TI-V is occurred through spin orbit coupling of Bi-p states. However, the band inversion of TI-C state is either created by the SOC, as in the case for Na, K, Rb, Cs or Mg based perovskites, or through weak but sensitive second neighbor Bi-p - Bi-p interactions as in the case for Ca, Sr and Ba based perovskites. Therefore, the family of TI perovskites can be classified into two based on the mechanism of band inversion.

II. STRUCTURAL AND COMPUTATIONAL DETAILS

We have studied the band structure of $ABiO_3$ in the cubic phase (space group Pm-3m) as shown in Fig. 1(a). The Wyckoff positions in the considered structure are 1a (0 0 0) for A, 1b (0.5 0.5 0.5) for Bi and 3c (0.5 0.5 0) for O ions. The salient features of the cubic structure are: (i) BiO_6 forms a perfect octahedral complex and (ii) the crystal structure has alternately stacked AO and BiO_2 planes. To study the surface states, we have constructed slabs along 001 as illustrated in Fig. 1(b). Both top and bottom surfaces are terminated with AO planes. The band structures are examined as a function of slab thickness to examine the evolution of the TI states and possible interactions between them.

The density functional calculations are carried out using the full potential linearized augmented plane wave (FP-LAPW) formalism [23] as implemented in WIEN2k simulation package [25]. Augmented plane waves in the interstitial and localized orbitals within the muffin-tin sphere are used to construct the basis sets. The largest vector in the plane wave expansion is obtained by setting RK_{max} to 7.0. The PBE-GGA exchange-correlation functional is used to solve the Kohn-Sham equations [26]. To carry out the Brillouin-zone integration $10 \times 10 \times 10$ k-mesh yielding 35 irreducible k-points, is used for the bulk structure and a proportionate k-mesh is used for the slab calculation.

III. BULK ELECTRONIC STRUCTURE OF $ABiO_3$

The chemical bonding, be it charge transfer (ionic) or sharing (covalent), plays a significant role in deciding the transport properties of a given solid. In most of the reports on Bi based alloy topological insulators, such as tellurides and selenides [14], the nature of chemical bonding has not been emphasized adequately while explaining the formation of TI states. It is due to the fact that these family of compounds are extensively studied in the past in the context of thermoelectric behavior and the presence of Bi-s and -p states at the Fermi level is well understood. However, the nature of chemical bonding in Bi based perovskites cannot be overlooked. Firstly because the TI state does not occur at E_F and hence its formation needs to be understood. Secondly, the perovskite

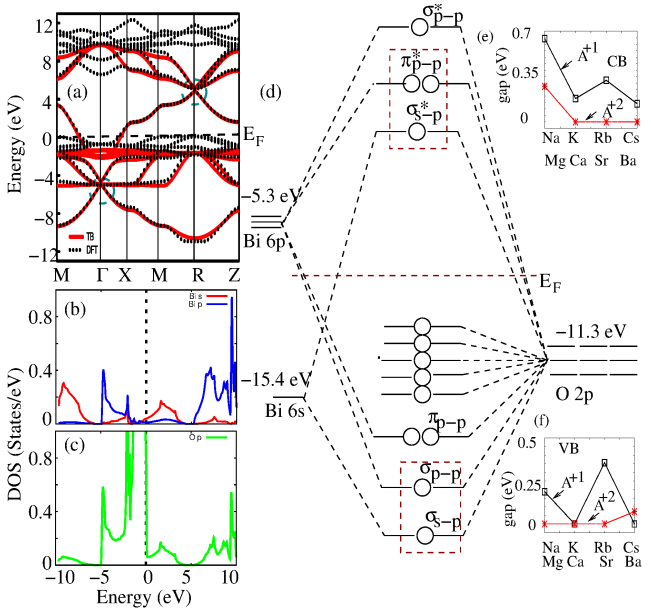

FIG. 2. Bulk electronic structure of $KBiO_3$, in the absence of SOC, illustrated through (a) band structure, (b and c) partial densities of states and (d) schematic molecular orbital picture (MOP). The band structure is obtained from both DFT (black dashed lines) and exact diagonalization of the TB Hamiltonian (red solid lines). In MOP diagram, $\{\sigma, \pi\}$ and $\{\sigma^*, \pi^*\}$ respectively represent the bonding and antibonding states which are resulted from the nearest neighbor Bi-$\{s, p\}$ - O-p covalent hybridization. Each member of $ABiO_3$ has similar electronic structure except the fact that there is a upward shift in E_F as the charge state of A changes from +1 to +2. The anti-bonding states σ^*_{s-p} and π^*_{p-p} either touche each other or open a gap between them depending on A as shown in (e). Similarly, the bonding states σ_{s-p} and σ_{p-p} either touche each other or open a gap between them depending on A as shown in (f).

has a BiO_6 octahedral complex which creates strong coordinated covalent interactions. As a consequence, the electronic structure exhibits highly dispersive bands that are very different from that of the Bi alloys [27, 28].

In this section, we analyse the electronic structure and chemical bonding mechanism of $ABiO_3$ using DFT and TB calculations. We take $KBiO_3$ as a prototype and extend the understanding to the other members of the family.

A. Electronic Structure of $KBiO_3$

Bulk electronic structure of $KBiO_3$ can be best explained from Fig. 2, where the band structure, orbital projected DOS and the resulted (schematic) molecular orbital picture for this compound are shown. The DFT band structure (Fig. 2(a), black dashed lines) suggests that this metallic system has two sets of four highly dispersive states - one lies in the conduction band and the other lies in the valence band. The highly dispersive states of the conduction band nearly touch each other at the high symmetry point R as marked with dotted circle. The orbital projected DOS infers that the lower lying band is primarily of Bi-s character and the remaining three bands are primarily of Bi-p character. Similarly, in the valence band, the dispersive states nearly touch each other at Γ with the lower band being Bi-s and upper bands being Bi-p in nature. Though similar feature has been reported in the earlier studies [18], the separation between the dispersive states of the conduction band and valence band which can be as large as 10 eV has not been analyzed and understood. Such exceptionally large separation, which is not observed in other Bi based TI families [27, 28] can only happen provided there is a strong covalent interaction making a set of bonding dispersive states lying lower in energy and a set of antibonding dispersive states lying higher in energy. Since, intra-site orbital overlap cannot exist, the interaction between Bi-s and Bi-p states is ruled out. On the contrary, due to the symmetric BiO_6 octahedra, stronger interaction is expected between the Bi-{s,p} and O-{p} states. Indeed the partial DOS, plotted in Fig. 2(c), shows significant presence of O-p characters everywhere in the energy spectrum.

In order to quantify the covalent interaction between the Bi-{s, p} and O-p states we have constructed a tight-binding model Hamiltonian with minimal basis set and is based on LCAO as adopted by Slater and Koster [24].

The Hamiltonian, which also includes SOC, is expressed as:

$$H = \sum_{i,\alpha} \epsilon_{i\alpha} c^\dagger_{i\alpha} c_{i\alpha} + \sum_{ij;\alpha,\beta} t_{i\alpha j\beta} (c^\dagger_{i\alpha} c_{j\beta} + h.c) + \lambda \mathbf{L}\cdot\mathbf{S} \quad (1)$$

Here i and j are the site indices while α and β are the orbitals forming the basis set. The latter consists of Bi s and p orbitals and O-p orbitals. The parameters $\epsilon_{i\alpha}$ and $t_{i\alpha j\beta}$ respectively represent the on-site energy and hopping integrals. In addition to the nearest neighbor Bi-O interactions, the second neighbor Bi-Bi interactions are included in the Hamiltonian. A similar TB model was adopted earlier to examine the superconducting Fermi surface of $BaBiO_3$ [29]. The third term of the Hamiltonian represents spin-orbit coupling (SOC) among the Bi-p states with coupling strength λ. Further details of the TB model, e.g. Hamiltonian matrix, optimized values of $t_{i\alpha j\beta}$, and SOC strength λ, are presented in appendix-I.

The Hamiltonian is exactly diagonalized and the resulted band dispersion is fitted with the one obtained from DFT. For $KBiO_3$ the TB bands in the absence of SOC are plotted in red solid lines in Fig. 2(a). We find excellent agreement between the TB bands and the two sets of highly dispersive (HD) bands. In fact at Γ and R, the DFT and TB bands coincide. For $KBiO_3$ the values of nearest neighbor (NN) hopping interaction strengths $V^{BiO}_{sp\sigma}$, $V^{BiO}_{pp\sigma}$ and $V^{BiO}_{pp\pi}$ are found to be 2.1, 2.95 and -0.75 eV respectively. The value of next nearest neighbor (NNN) hopping interaction strengths $V^{BiBi}_{ss\sigma}$,

$V_{sp\sigma}^{BiBi}$, $V_{pp\sigma}^{BiBi}$ and $V_{pp\pi}^{BiBi}$ are found to be -0.04, 0.02, -0.08 and 0.16 eV respectively. Similar results are obtained for other members and details are listed in Table-I of appendix-I.The electronic structure and chemical bonding in the family of $ABiO_3$ as inferred from the DFT and TB calculations are summarized in the molecular orbital picture (MOP) shown in Fig. 2(d). The cation A transfers its valence electrons to the anion O and does not take part in the bonding. However, Bi remains in an ambiguous charge state since electrons from the outer Bi-s orbitals, with -15.4 eV atomic on-site energy, cannot be transferred to O-p states which are at higher on-site energy of -11.3 eV. Therefore, electron sharing occurs between Bi and O through strong covalent interaction between them. The Bi-s - O-p interaction creates a bonding state σ_{s-p} and an antibonding state σ^*_{s-p}. Similarly, the Bi-p - O-p interactions create a set of bonding states $\{\sigma_{p-p}, \pi_{p-p}\}$ and a set of antibonding states $\{\sigma^*_{p-p}, \pi^*_{p-p}\}$ as shown in the Fig. 2(d). The bonding states σ_{s-p} and σ_{p-p} either touch each other, to create accidental degeneracy, or open a gap between them depending on the cation A (see Fig. 2(f)). Similarly the anti-bonding states σ^*_{s-p} and π^*_{p-p} either touch each other or open a gap between them depending on A as shown in Fig. 2(e). As a consequence, there is a possibility of two TI states, one in the valence band (VB) and the other in the conduction band (CB), in the family of $ABiO_3$.

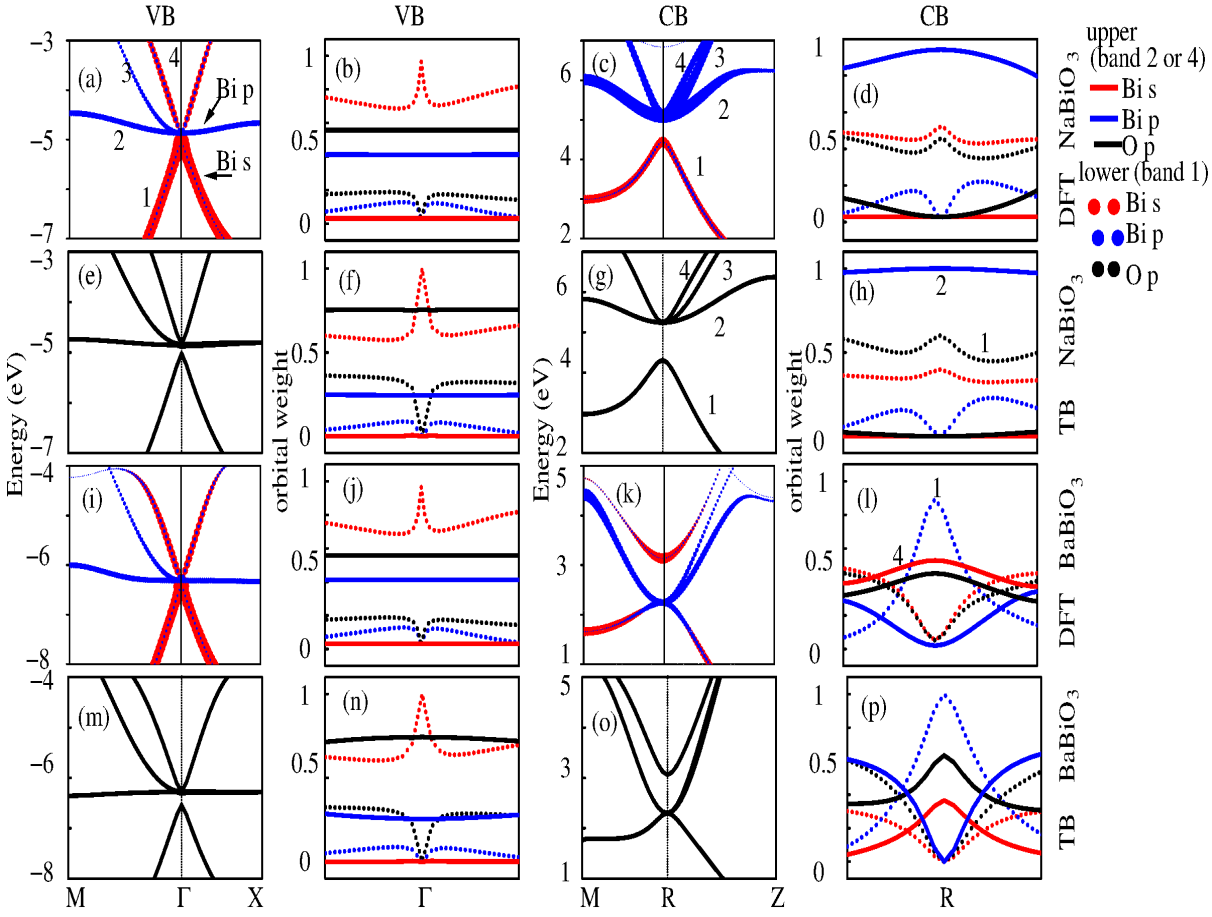

FIG. 3. DFT and TB obtained valence bands along M-Γ-X (first column) and conduction bands along M-R-Z (third column) for $NaBiO_3$ and $BaBiO_3$ in the absence of SOC. The DFT bands are shown with projected orbital characters. Right to each band structure the orbital weights (contribution of individual orbitals in forming a band) of the relevant bands, responsible for constructing the topologically invariant surface states, are shown. For the valence spectrum, the relevant ones are band-1 and 2. For the conduction spectrum, the relevant ones are band-1 and 2 for $NaBiO_3$ and band-1 and 4 for $BaBiO_3$. For the orbital weight plots, the solid lines represent the upper band (2 or 4) and dotted lines represent the lower band (band-1). Interestingly for Ba based compound, band-1 and 4 reverse their characters at R which suggests that a band inversion already exists due to hybridization. The band structures of $KBiO_3$, $RbBiO_3$, $CsBiO_3$ and $MgBiO_3$ resemble to that of $NaBiO_3$ and constitute one class of topological insulator where SOC leads to band inversion. The band structures of $CaBiO_3$ and $SrBiO_3$ resembles to that of $BaBiO_3$ and constitute the other class of topological insulator where the band inversion occurs through hybridization.

The MOP is nearly similar for each member of $ABiO_3$. To avoid the repetition, we have shown the band structure of these compounds (other than $KBiO_3$) in appendix-II. However, in the coming sections we will see that even though the NNN Bi-Bi hoping interaction strengths are weak, a minor variation of them can lead to different mechanism for forming the TI states in the conduction band.

B. Hybridization Induced Band Inversion and Classification of $ABiO_3$ compounds

The broad picture of electronic structure of $ABiO_3$ presented in Fig. 2 is inadequate to evolve a mechanism for the formation of TI surface states in this family. We need to investigate the local variation in the valence band dispersion at the high symmetry point Γ and conduction band dispersion at the high symmetry point R and also identify the orbitals constructing these bands. Therefore, in Fig. 3 we have plotted the DFT and TB obtained conduction bands along M-R-Z and valence bands along M-Γ-X for $NaBiO_3$ and $BaBiO_3$. These two compounds are chosen as prototypes to represent the compounds with A^{+1} and A^{+2} cations. The orbital projected band structure (orbital contribution to a given band is proportional to thickness of the curve shown), obtained from DFT, shows that the valence bands for both the compounds are nearly exact with the lower lying band (band-1) is predominantly of Bi-s and the upper two weakly disperse bands (band-2, 3) are of Bi-p character. The uppermost highly dispersive band (band-4) is occupied by Bi-s orbital in the vicinity of Γ, however, in rest part of the Brillouin zone (not shown here) it is more dominated by Bi-p characters. We may note that since the formation of these states are based on their covalent interactions between the Bi-$\{s, p\}$ and O-$\{p\}$ states (see Fig. Fig. 2(d), MOP) the O-p contribution is significant in all these bands.

From the analysis of the band dispersion and orbital weight factor, we find that in the case of conduction bands, there is a clear distinction between $NaBiO_3$ (Figs. 3 (c,d DFT) and (g,h TB)) and $BaBiO_3$ (Figs. 3(k,l DFT) and (o,p TB)). For the former, at the high symmetry point R, the lower band, is occupied by Bi-s, while the upper three bands are occupied by Bi-p characters. On the contrary for the latter, the lower band is of Bi-p character while the uppermost band (band-4) is of Bi-s character. Therefore, it suggests that there is a hybridized induced band inversion in $BaBiO_3$ between the lower band and the uppermost band. In addition to $BaBiO_3$, the orbital weights listed in Table-III of appendix-II suggests similar band structure in the case of $CaBiO_3$ and $SrBiO_3$. Interestingly a very recent article [22] suggests identical hybridization band inversion in A_2BiXO_6, where A being Ca, Sr and Ba and X being Br or I. This carries significance as in most of the Bi based topological insulators, the band inversion occurs only through spin orbit coupling.

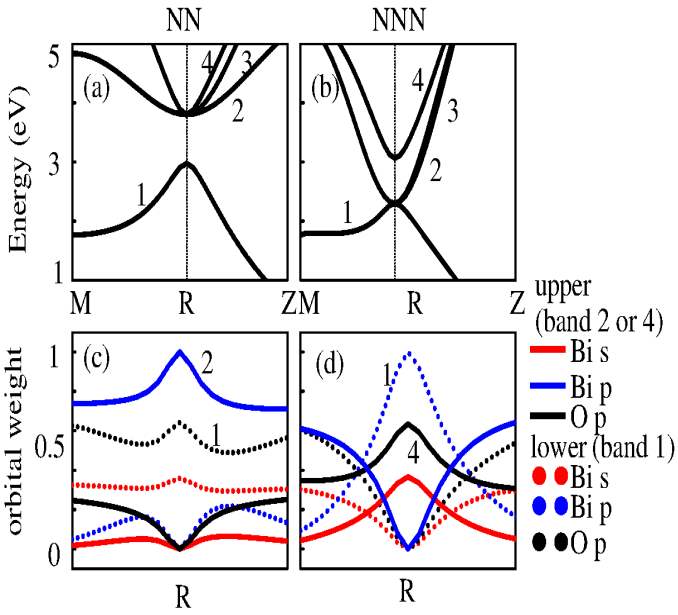

FIG. 4. (First row) TB obtained $ABiO_3$ conduction band structure along the Brillouin zone path M-R-Z: (a) when the interactions are restricted to nearest neighbor (NN) only and (b) when the interactions include next nearest neighbors (NNN). (second row) The orbital weights in the vicinity of R for the corresponding bands shown in the first row. The solid lines show the orbital weights for the upper bands (2 or 4) and dashed lines represent the same for the lower band (band-1)

To provide a quantitative picture of hybridized band inversion, both our DFT (Fig. 3(l)) and TB (Fig. 3(p)) calculations show that away from R, the band-1 (lower band) is composed of 40% Bi-s and 60% O-p character. But at R, the band is completely formed by Bi-p orbitals. In the case of band-4 (uppermost band) it is reversed. Away from R, the band is composed of 60% Bi-p and 40% O-p states. At R it is composed of 40% Bi-s and 60% O-p. This establishes the Bi s-p band inversion at R in $BaBiO_3$. The valence bands of both the compounds appear similar and no band inversion is observed between band-1 and 2 as in the case of conduction bands of $NaBiO_3$.

The calculation of orbital weights also shows that there is a significant presence of O-p characters in the conduction and valence dispersive bands which in turn implies that in pervoskites, unlike the selenides and tellurides, the hybridized states, instead of pure Bi states, construct the TI states.

The cause of hybridized induced band inversion in $BaBiO_3$ and absence of it in $NaBiO_3$ can be explained using the tight-binding model. In Fig. 4, we have plotted the conduction band structure of $ABiO_3$, around the high symmetry point R, and the orbital weight factors in these bands for two cases. In the first case, we switched off the next nearest neighbor interactions (Bi-Bi) and only

nearest neighbor Bi-O interactions are included in the TB Hamiltonian. The resulted band structure as well as the plot of k-dependent orbital weights (Figs. 4(a) and (c)) resemble to that of $NaBiO_3$ (see Figs. 3(g) and (h)). However, when the NNN Bi-Bi interactions are included in the Hamiltonian, the resulted band structure as well as the plot of the orbital weights (Figs. 4(b) and (d)) resemble to that of the $BaBiO_3$ (see Figs. 3(o) and (p)). This suggests that the second neighbor interactions induce the s-p band inversion. From the optimized TB parameters listed in Table-I of appendix-I, we find that the second neighbor interactions, particularly the ppσ and ppπ, are significant in $CaBiO_3$, $SrBiO_3$ and $BaBiO_3$. Accordingly, in the absence of SOC, the s-p band inversion occurs in these compounds while the rest of the compounds do not have it.

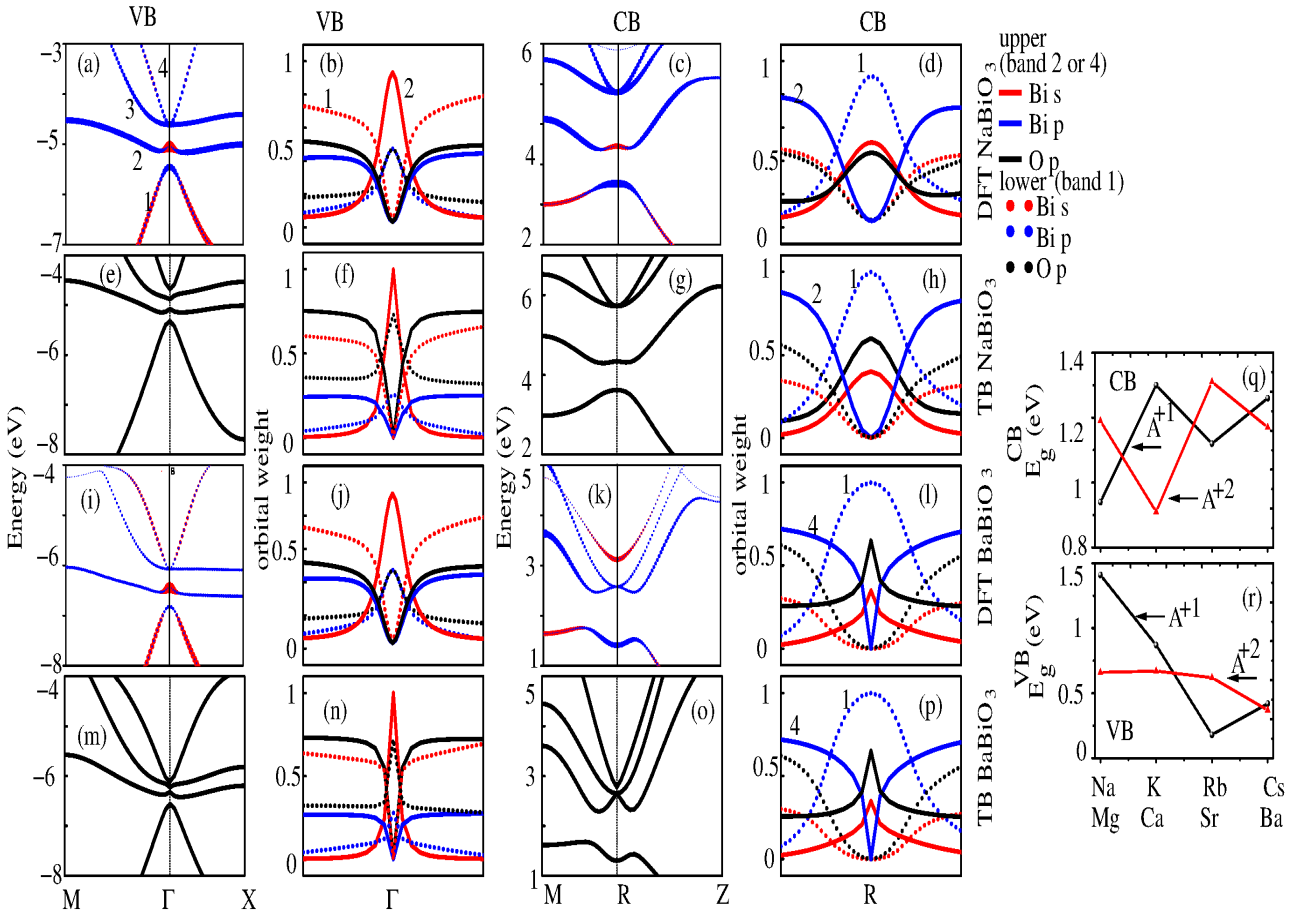

FIG. 5. DFT+SOC and TB+SOC obtained valence bands along M-Γ-X (first column) and conduction bands along M-R-Z (third column) for $NaBiO_3$ and $BaBiO_3$. The DFT bands are shown with projected orbital characters. Right to each band structure the orbital weights of the relevant bands are shown. The solid lines represent the upper band (2 or 4) and dotted lines represent the lower band (band-1). With inclusion of SOC, the band inversion occurs between the band-1 and 2 in the valence band of both the compounds and in the conduction band of $NaBiO_3$. The hybridized induced s-p band inversion in the conduction spectrum of $BaBiO_3$ remains unaffected by SOC. The SOC either creates a gap or amplifies the already existing gap at R in the conduction band (E_g^{CB}) and at Γ in the valence band (E_g^{VB}). (q) and (r) plot (E_g^{CB}) and (E_g^{VB}) respectively for different A cations.

C. Effect of spin-orbit coupling

Having understood the electronic structure due to chemical bonding through Figs. 2, 3 and 4, in this section we shall discuss the effect of spin orbit coupling of the Bi-p states on the band structure. Fig. 5 shows the DFT+SOC and TB+SOC band structures as well as k-dependent orbital weights of the relevant bands for

$NaBiO_3$ and $BaBiO_3$. SOC introduces two significant changes in the band structure at the high symmetry point Γ in the valence band and at the high symmetry point R in the conduction band. Firstly either a gap appears at these points or the already existing gap (see Figs. 2(e) and (f)) gets amplified except in the case of $RbBiO_3$. The magnitude of the gap at Γ (E_g^{VB}) and at R (E_g^{CB}) as a function of A cation is shown in Figs. 5(q) and (r) respectively. For $RbBiO_3$, the chemical bonding resulted E_g^{VB} reduced from 0.35 eV to 0.2 eV due to SOC. However, the gap remains robust. Secondly, from the calculations of orbital weights, the band-1 and 2 of valence band alter their characters at Γ. For example, according to our TB calculations on $NaBiO_3$, without SOC (see Fig. 3(f)), at Γ band-1 is composed of Bi-s character only and band-2 is composed of 25% Bi-p and 75% O-p characters. With the inclusion of SOC (see Fig. 5(f)), the band-1 is now composed of 27% Bi-p and 73% O-p characters, whereas band-2 is solely made up of Bi-s states. The DFT calculations provide similar results as can be seen from Figs. 3(b) and 5(b). Band-1 and 2 of the conduction band (for A = Na, K, Rb, Cs and Mg) also undergo similar inversion at R. Table-IV of appendix-II, lists the orbital weights at Γ and *R* for band-1 and 2 to reconfirm the band inversion in these compounds. The hybridization induced band inversion in the conduction band of $BaBiO_3$, $CaBiO_3$ and $SrBiO_3$ remains unaffected by SOC. By fitting the TB+SOC bands with that of the DFT+SOC obtained bands, we found that the SOC strength for the latter three compounds is about 0.5 eV which is nearly 0.2 eV smaller compared to that of the other members of the family.

IV. SURFACE ELECTRONIC STRUCTURE OF $ABiO_3$

The hallmark of topological insulators is the formation of a Dirac type surface state within the bulk band gap created by SOC. Such a state is invariant under adiabatic deformation. As bulk $ABiO_3$ exhibit two SOC induced bulk band gaps (E_g^{VB} and E_g^{CB}) it is imperative to see whether this perovskite family forms two such Dirac type surface states protected by symmetry.

These surface states are primarily examined by solving the TB model Hamiltonians with minimal basis set instead of a full-basis set based DFT study [17, 19]. In most of the cases, the minimal Wannier basis are obtained from the bulk electronic structure and subjected to the TB Hamiltonian to obtain the k-dependent eigenstates. In such studies while the surface confinement is well taken into account, the microscopic changes in the chemical bonding, which lead to significant changes in the surface states, are often ignored. Therefore, in this section we present the surface electronic structure calculated using the full potential linearized augmented plane wave method where both plane waves and local orbitals form the basis.

Furthermore, recent reports suggest that not necessarily all the films of well established topological insulators exhibit Dirac like surface states. From the ARPES study it is found that in ultra thin Bi_2Se_3 (three quintuple layers and less), there is an energy gap that appears between the topological surface state bands [30]. The first principles calculations infer similar conclusions in the case of Bi_2Te_3 films [31]. Keeping this in mind we have examined the robustness of the surface state as a function of film thickness.

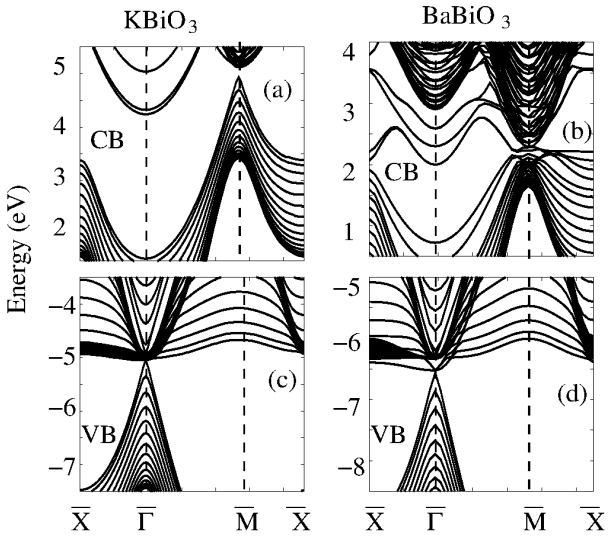

FIG. 6. Valence and conduction band structure of 15 unit cell thick $KBiO_3$ and $BaBiO_3$ in the absence of SOC

First, to examine the effect of chemical bonding, we shall analyze surface electronic structure without SOC. To make the point, the band structure of 15 unit cell thick $KBiO_3$ and $BaBiO_3$ slabs are shown in Fig. 6. The figure suggests that while the bulk valence band gap at Γ ($\bar{\Gamma}$) and bulk conduction band gap at R (in the surface Brillouin zone R is mapped to $\bar{M}$) are either reduced or disappeared completely in this slab, there is no signature of Dirac type bands appearing at $\bar{\Gamma}$ and $\bar{M}$ of the surface Brillouin zone. Therefore, the hybridized induced band inversion has minimal role in forming the TI surfaces states.

To investigate the role of SOC, in Fig. 7, we have plotted the DFT+SOC band structure of $KBiO_3$ and $BaBiO_3$ films of 15 unit cell thick. From the figure we find that linearly dispersed bands, akin to the TI states, appear within the bulk gap. The layer and atom resolved orbital weights of these linear bands estimated at $\bar{M}$ or $\bar{\Gamma}$ (see Figs. 7(c) and (d) for $KBiO_3$; (g) and (h) for $BaBiO_3$) imply that these linear bands are made up of surface O-p, Bi-s and Bi-p states. As we move from the surface to the interior, the contribution rapidly vanishes and three layers below the surface, the contribution to these linear bands ceases to exist. Therefore, these linear bands are well defined surface states and satisfy all the

criteria to be called as TI states. The surface TI states of each member of this family are shown in appendix-II.

The robustness of the surface TI states can be measured based on two factors: (i) its invariance with adiabatic deformation [32] and (ii) its invariance with respect to the thickness of the film. While the former has been proved based on parity of the bands and calculation of Chern numbers (Z_2), the latter is purely a function of chemical bonding which has not been highlighted yet for the family of perovskites. The band structure of five unit cell thick $RbBiO_3$, shown in Figs. 8(a) and (b) reveals that the conduction linear bands at $\bar{M}$ give rise to a gap (E_g^{CS}) of 0.17 eV. Similarly the valence linear bands at $\bar{\Gamma}$ give rise to a gap (E_g^{VS}) of 0.45 eV. Both of these gaps lie well within the SOC driven bulk band gaps. Furthermore, from the layer resolved orbital decomposition (not shown here) we find that the bands below and above of these new energy gaps are formed by the orbitals of the surface layers. This implies the presence of a strong interaction between the bottom and top surface states which gives rise to these gaps. To provide a quantitative measure, in Fig. 8(c-f)we have plotted E_g^{VS} and E_g^{CS} as function of film thickness. As expected, we find that the gap sharply decreases with increasing thickness. However, the critical thickness below which the gap vanishes, varies with the cation A. Also for a given compound the critical thickness differs for E_g^{VS} and E_g^{CS}. With increase in the thickness of the slab, the separation between the bottom and top surfaces increases and thereby the coupling between the surface states vanishes to create two non-interacting TI Dirac bands.

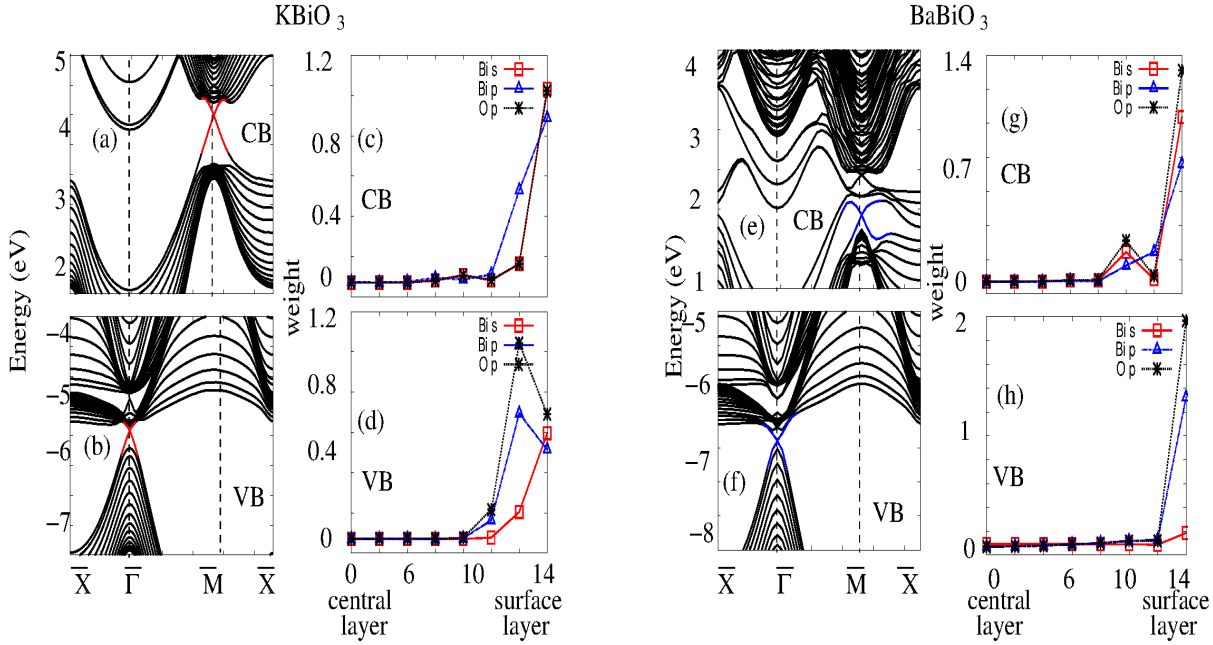

FIG. 7. Surface conduction and valence band structure along $\bar{X}$-$\bar{\Gamma}$-$\bar{M}$-$\bar{X}$ for 15 unit cell thick $KBiO_3$(a and b) and $BaBiO_3$(e and f). Dirac type linear bands appear between the gap opened up by SOC. Figures (c) and (d), for $KBiO_3$, and (g) and (h), for $BaBiO_3$, show the layer and atom resolved orbital weights of conduction and valence linear bands at $\bar{M}$ and $\bar{\Gamma}$ respectively for $KBiO_3$. Here we gather that orbitals of first three to four layers from the surface constitute these linear bands.

V. SUMMARY AND CONCLUSION

To summarize, bulk and surface electronic structure of $ABiO_3$ family, where A is either a monovalent (Na, K, Rb and Cs) or a divalent (Mg, Ca, Sr and Ba) element, are obtained from DFT calculations and from exact diagonalization of a minimal basis based TB Hamiltnian. Existence of two topologically invariant (TI) surface Dirac states, one in the conduction band and other in the valence band, is the characteristic feature of this family. The valence TI state arises from the bonding interaction between Bi-{s,p} - O-{p} states in the BiO_6 octahedral complex. The corresponding antibonding interaction constitutes the conduction TI state. While the spin orbit coupling (SOC) induces s-p band inversion in the valence band, in the case of conduction band, the inver-

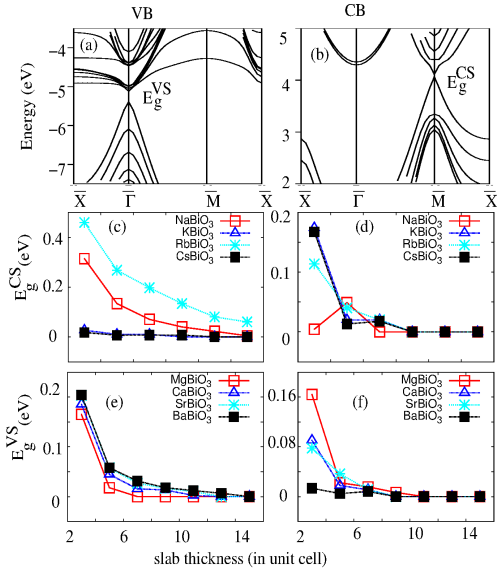

FIG. 8. Valence (a) and conduction (b) band structure for 5 unit cell thick $RbBiO_3$ demonstrating the existence of a band gap between the topological surface states both in conduction (E_g^{CS}) and valence band spectrum (E_g^{VS}). The surface energy gap lies between the SOC induced bulk band gap (E_g^{VB} or E_g^{CB}). Figures (c) and (d) plot the variation of E_g^{CS} and E_g^{VS} as a function of film thickness for $ABiO_3$ when A is in +1 charge state (Na, K, Rb, and Cs). Figures (e) and (f) are same as (c) and (d) but when A is in +2 charge state (Mg, Ca, Sr and Ba).

sion is induced either through SOC or through the weak but sensitive second neighbor hybridization between the Bi states. Therefore, this perovskite family can be classified into two, with one class (A = Na, K, Rb, Cs and Mg) follows the SOC mechanism and the other (A = Ca, Sr and Ba) follows the hybridization mechanism for the inversion of Bi-s and p characters in the conduction band. The top and bottom surface TI states of $ABiO_3$ can couple to destroy their Dirac type linear dispersion. The critical thickness (C_T, above which the coupling ceases to exist, vary with A and lie in the range 4 to 14 unit cell. C_T is also different for conduction and valence surface states. The mechanisms of band inversion and formation of more than one TI surfaces, proposed in this work, can be extended to other complex oxides where the heavy elements like Bi and Pb form symmetric oxygen complexes.

Acknowledgments: The authors acknowledge the computational resources provided by HPCE, IIT Madras.

VI. APPENDIX-I: TIGHT-BINDING MODEL

The basis set for the TB Hamiltonian Eq.1 consists of the one Bi-s, three Bi-p and the nine O-p (three per each oxygen anion) orbitals. The rest are neglected as they neither lie in the vicinity of the Fermi level nor participate in the formation of the topological invariant states. Also the hopping interactions are confined to the nearest neighbor and next nearest neighbor coordination except the case of O. This is due to the fact that O-p - O-p interaction is not significant in forming the highly dispersive states at Γ in the valence band and at R at the conduction band. Therefore, TB Hamiltonian matrix, constructed with the help of Slater-Koster hopping integrals (SKI) [24], includes Bi-s - O-p and Bi - Bi interactions. The relevant SKIs are reproduced here.

$$\begin{aligned} E_{s,x} &= lt_{sp\sigma} \\ E_{x,x} &= l^2 t_{pp\sigma} - (1-l^2) t_{pp\pi} \\ E_{x,y} &= lmt_{pp\sigma} - lmt_{pp\pi} \\ E_{x,z} &= lnt_{pp\sigma} - lnt_{pp\pi}, \end{aligned} \tag{2}$$

where, x, y and z represent p_x, p_y and p_z orbitals respectively and l, m, n are direction cosines. The parameter t quantify the covalent interactions of various types (σ and π).

The spin independent TB Hamiltonian matrix, with the basis set in the order $\{|s^{Bi}\rangle\ |p_x^{Bi}\rangle, |p_y^{Bi}\rangle, |p_z^{Bi}\rangle\ |p_x^{O1}\rangle, |p_y^{O1}\rangle, |p_z^{O1}\rangle, |p_x^{O2}\rangle, |p_y^{O2}\rangle, |p_z^{O2}\rangle, |p_x^{O3}\rangle, |p_y^{O3}\rangle, |p_z^{O3}\rangle\}$, takes the form:

$$H = \begin{pmatrix} M_{4\times4}^{Bi-Bi} & M_{4\times9}^{Bi-O} \\ M_{4\times9}^{Bi-O\dagger} & M_{9\times9}^{O-O} \end{pmatrix} \tag{3}$$

$$M_{4\times4}^{Bi-Bi} = \begin{pmatrix} \epsilon_s + f_1 & 2it_{sp\sigma}^{Bi-Bi}\sin(k_x a) & 2it_{sp\sigma}^{Bi-Bi}\sin(k_y a) & 2it_{sp\sigma}^{Bi-Bi}\sin(k_z a) \\ -2it_{sp\sigma}^{Bi-Bi}\sin(k_x a) & \epsilon_{p1} + f_2 & 0 & 0 \\ -2it_{sp\sigma}^{Bi-Bi}\sin(k_y a) & 0 & \epsilon_{p1} + f_3 & 0 \\ -2it_{sp\sigma}^{Bi-Bi}\sin(k_z a) & 0 & 0 & \epsilon_{p1} + f_4 \end{pmatrix} \tag{4}$$

$$M_{4\times9}^{Bi-O} = \begin{pmatrix} t_{sp\sigma}^{Bi-O}S_x & 0 & 0 & 0 & t_{sp\sigma}^{Bi-O}S_y & 0 & 0 & 0 & t_{sp\sigma}^{Bi-O}S_z \\ t_{pp\sigma}^{Bi-O}C_x & 0 & 0 & t_{pp\pi}^{Bi-O}C_y & 0 & 0 & t_{pp\pi}^{Bi-O}C_z & 0 & 0 \\ 0 & t_{pp\pi}^{Bi-O}C_x & 0 & 0 & t_{pp\sigma}^{Bi-O}C_y & 0 & 0 & t_{pp\pi}^{Bi-O}C_z & 0 \\ 0 & 0 & t_{pp\pi}^{Bi-O}C_x & 0 & 0 & t_{pp\pi}^{Bi-O}C_y & 0 & 0 & t_{pp\sigma}^{Bi-O}C_z \end{pmatrix} \quad (5)$$

$$M_{9\times9}^{O-O} = \begin{pmatrix} \epsilon_{p2} & 0 & 0 & 0 & 0 & 0 & 0 & 0 & 0 \\ 0 & \epsilon_{p2} & 0 & 0 & 0 & 0 & 0 & 0 & 0 \\ 0 & 0 & \epsilon_{p2} & 0 & 0 & 0 & 0 & 0 & 0 \\ 0 & 0 & 0 & \epsilon_{p2} & 0 & 0 & 0 & 0 & 0 \\ 0 & 0 & 0 & 0 & \epsilon_{p2} & 0 & 0 & 0 & 0 \\ 0 & 0 & 0 & 0 & 0 & \epsilon_{p2} & 0 & 0 & 0 \\ 0 & 0 & 0 & 0 & 0 & 0 & \epsilon_{p2} & 0 & 0 \\ 0 & 0 & 0 & 0 & 0 & 0 & 0 & \epsilon_{p2} & 0 \\ 0 & 0 & 0 & 0 & 0 & 0 & 0 & 0 & \epsilon_{p2} \end{pmatrix} \quad (6)$$

TABLE I. Tight binding parameters without soc calculation

charge	A	E_{Bi-s}	E_{Bi-p}	E_{O-p}	t_{sp}	$t_{sp\sigma}$	$t_{pp\pi}$	t_{ss}^{Bi-Bi}	$t_{sp\sigma}^{Bi-Bi}$	$t_{pp\sigma}^{Bi-Bi}$	$t_{pp\pi}^{Bi-Bi}$
+1	Na	-4.78	5.32	-1.55	2.08	2.75	-0.7	-0.04	0.06	-0.12	0.08
	K	-4.4	5.7	-1.6	2.1	2.95	-0.75	-0.04	0.02	-0.08	0.16
	Rb	-4.6	5.5	-1.5	2.1	2.8	-0.7	-0.03	0.07	-0.01	0.16
	Cs	-5	5.1	-1	2.1	2.8	-0.75	-0.07	0.11	-0.14	0.2
+2	Mg	-6.6	3.5	-2.5	2.1	2.75	-0.85	-0.02	-0.0	-0.05	0.04
	Ca	-6.6	3.5	-2.5	2.1	2.8	-1.4	-0.04	-0.04	-0.1	0.55
	Sr	-6.5	3.6	-2.4	2	2.7	-1.35	-0.04	-0.08	-0.22	0.45
	Ba	-6.63	3.47	-2.57	2	2.82	-1.35	-0.04	-0.16	-0.25	0.5

TABLE II. Tight binding parameters soc calculation

charge	A	E_{Bi-s}	E_{Bi-p}	E_{O-p}	t_{sp}	$t_{sp\sigma}$	$t_{pp\pi}$	t_{ss}^{Bi-Bi}	$t_{sp\sigma}^{Bi-Bi}$	$t_{pp\sigma}^{Bi-Bi}$	$t_{pp\pi}^{Bi-Bi}$	λ
+1	Na	-4.78	5.32	-1.55	2.08	2.61	-0.9	-0.05	-0.05	-0.05	0.1	0.7
	K	-4.4	5.7	-1.6	2.15	2.82	-0.7	-0.05	-0.05	-0.05	0.15	0.7
	Rb	-5.4	4.7	-0.5	2.08	2.9	-1.15	0.07	0.05	-0.05	0.1	0.6
	Cs	-4.9	5.2	-0.8	2	3	-0.85	-0.02	-0.12	-0.15	0.25	0.7
+2	Mg	-6.6	3.5	-2.5	2.1	2.75	-1.3	0.02	0.05	-0.4	0.3	0.7
	Ca	-6.6	3.5	-2.6	2	2.75	-1.5	-0.03	0.05	-0.3	0.5	0.5
	Sr	-6.4	3.7	-2.3	2.0	2.7	-1.5	-0.03	0.05	-0.3	0.5	0.45
	Ba	-6.63	3.47	-2.57	2	2.7	-1.3	0.03	0.05	0.3	0.2	0.45

Here ϵ_s, ϵ_{p1} and ϵ_{p2} are on-site energies of Bi-s, Bi-p and O-p orbitals respectively. The terms C_x and S_x are short notation for $2\cos(k_x a/2)$ and $2i\sin(k_x a/2)$ make the Hamiltonian k-dependent and f_i $(i = 1, 2, 3, 4)$ arises from Bi-Bi second neighbour interactions, are given by

$$\begin{aligned} f_1 &= 2t_{ss}^{Bi-Bi}(cos(k_x a) + cos(k_y a) + cos(k_z a)) \\ f_2 &= 2t_{pp\sigma}^{Bi-Bi}cos(k_x a) + 2t_{pp\pi}^{Bi-Bi}[cos(k_y a) + cos(k_z a)] \\ f_3 &= 2t_{pp\sigma}^{Bi-Bi}cos(k_y a) + 2t_{pp\pi}^{Bi-Bi}[cos(k_x a) + cos(k_z a)] \\ f_4 &= 2t_{pp\sigma}^{Bi-Bi}cos(k_z a) + 2t_{pp\pi}^{Bi-Bi}[cos(k_x a) + cos(k_y a)] \end{aligned} \quad (7)$$

The k-dependency arises through the Bloch summation:

$$h_{\alpha\beta}(k) = \sum_l t_{j\alpha l\beta} exp[i\vec{k}\cdot(\vec{R}_l - \vec{R}_j)], \quad (8)$$

where j and α respectively represent site and orbital indices and R_j is the position vector for j-th site. The terms $t_{j\alpha l\beta}$ are constructed from Eq. 2.

The SOC component of the Hamiltonian, acting on the Bi-p states, is expressed as:

$$H_{SOC} = \lambda \mathbf{L}\cdot\mathbf{S} \quad (9)$$

$$\begin{aligned}\langle L\cdot S\rangle &= \frac{1}{2}\langle J^2 - L^2 - S^2\rangle \\ &= \frac{\hbar^2}{2}(j(j+1) - l(l+1) - s(s+1))\end{aligned} \tag{10}$$

To operate the SOC Hamiltonian on the p-orbitals, we need to express them as a linear combination of total angular momentum states (Φ_{j,m_j}).

$$\begin{aligned}
p_x\uparrow &= \frac{1}{\sqrt{2}}\Big(\Phi_{\frac{3}{2},\frac{3}{2}} + \frac{1}{\sqrt{3}}\Phi_{\frac{3}{2},-\frac{1}{2}} + \sqrt{\frac{2}{3}}\Phi_{\frac{1}{2},-\frac{1}{2}}\Big)\\
p_y\uparrow &= -\frac{i}{\sqrt{2}}\Big(\Phi_{\frac{3}{2},\frac{3}{2}} - \frac{1}{\sqrt{3}}\Phi_{\frac{3}{2},-\frac{1}{2}} + \sqrt{\frac{2}{3}}\Phi_{\frac{1}{2},-\frac{1}{2}}\Big)\\
p_z\uparrow &= \sqrt{\frac{2}{3}}\Phi_{\frac{3}{2},-\frac{1}{2}} - \sqrt{\frac{1}{3}}\Phi_{\frac{1}{2},-\frac{1}{2}}\Big)\\
p_x\downarrow &= \frac{1}{\sqrt{2}}\Big(\frac{1}{\sqrt{3}}\Phi_{\frac{3}{2},\frac{1}{2}} + \sqrt{\frac{2}{3}}\Phi_{\frac{1}{2},\frac{1}{2}} + \Phi_{\frac{3}{2},-\frac{3}{2}}\Big)\\
p_y\downarrow &= -\frac{i}{\sqrt{2}}\Big(\frac{1}{\sqrt{3}}\Phi_{\frac{3}{2},\frac{1}{2}} + \sqrt{\frac{2}{3}}\Phi_{\frac{1}{2},\frac{1}{2}} - \Phi_{\frac{3}{2},-\frac{3}{2}}\Big)\\
p_z\downarrow &= \sqrt{\frac{2}{3}}\Phi_{\frac{3}{2},-\frac{1}{2}} + \sqrt{\frac{1}{3}}\Phi_{\frac{1}{2},-\frac{1}{2}}\Big)
\end{aligned} \tag{11}$$

With the aid of Eq. 10 and 11, we obtain the matrix elements for the SOC Hamiltonian with the basis set in the order: $|p_x^{Bi}\uparrow\rangle$, $|p_y^{Bi}\uparrow\rangle$, $|p_z^{Bi}\uparrow\rangle$, $|p_x^{Bi}\downarrow\rangle$, $|p_y^{Bi}\downarrow\rangle$, $|p_z^{Bi}\downarrow\rangle$

$$H_{SOC} = \lambda\begin{pmatrix} 0 & -i & 0 & 0 & 0 & 1\\ i & 0 & 0 & 0 & 0 & -i\\ 0 & 0 & 0 & 1 & -i & 0\\ 0 & 0 & 1 & 0 & i & 0\\ 0 & 0 & i & -i & 0 & 0\\ 1 & i & 0 & 0 & 0 & 0\end{pmatrix} \tag{12}$$

The Hamiltonian matrix is exactly diagonalized and the resulted band dispersion is fitted with that of DFT with RMS deviation tolerance less than 0.2. The optimized tight binding parameters in the absence of SOC are listed in Table-I and same in the presence of SOC is listed in Table-II. Table-II also lists the SOC strength λ. As expected, only the second neighbor Bi-Bi interaction parameters vary with inclusion of SOC.

VII. APPENDIX-II: ELECTRONIC STRUCTURE OF $ABiO_3$

To avoid repetition, the surface and bulk electronic structure of each member of the $ABiO_3$ family are not shown in the main text. They are presented here. The captions of the figures and the tables are complete and self explanatory.

And also orbital weight factors are listed in Table-III and Table-IV with and without SOC. From the tabulated data we conclude that the band inversion exist in all $ABiO_3$ compounds.

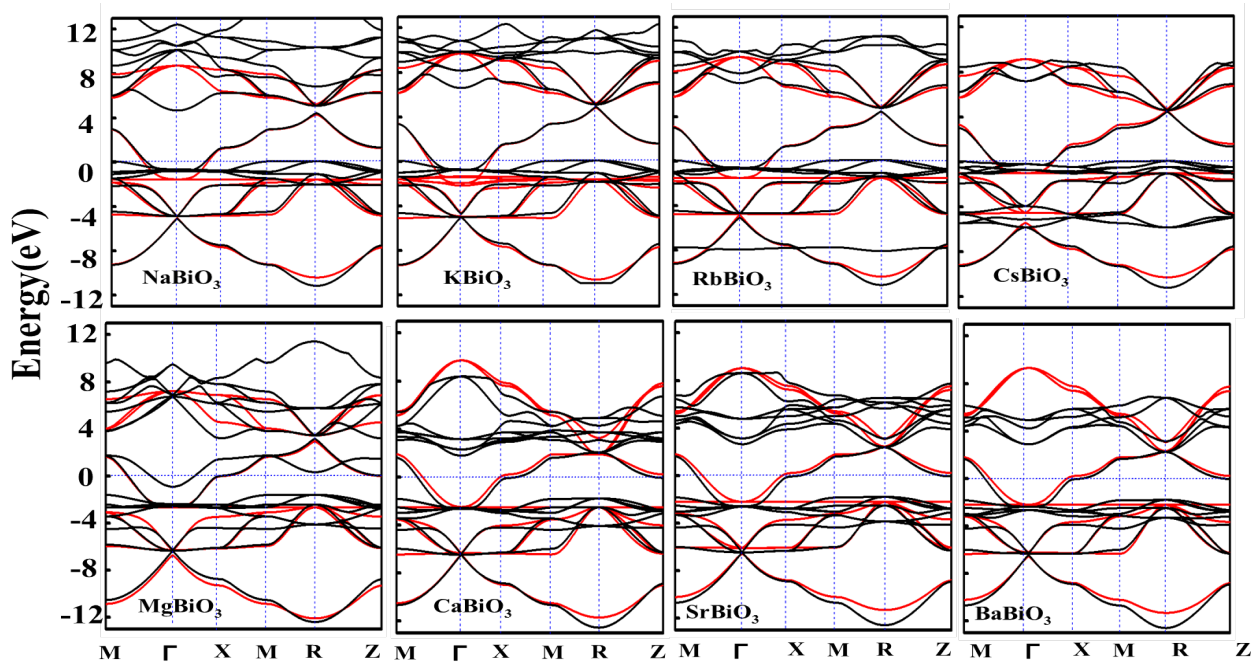

FIG. 9. Full bulk band structure of $ABiO_3$ in the absence of SOC. Black and red lines represent bands obtained from DFT and TB respectively. TB bands are composed of Bi-{s,p } and O-{p} orbitals. There is an excellent agreement between these two set of bands. As discussed in the main text, narrow (or vanishing) band gaps at Γ in the valence band and at R in the conduction band suggest the possibility of formation of two topologically invariant surface states.

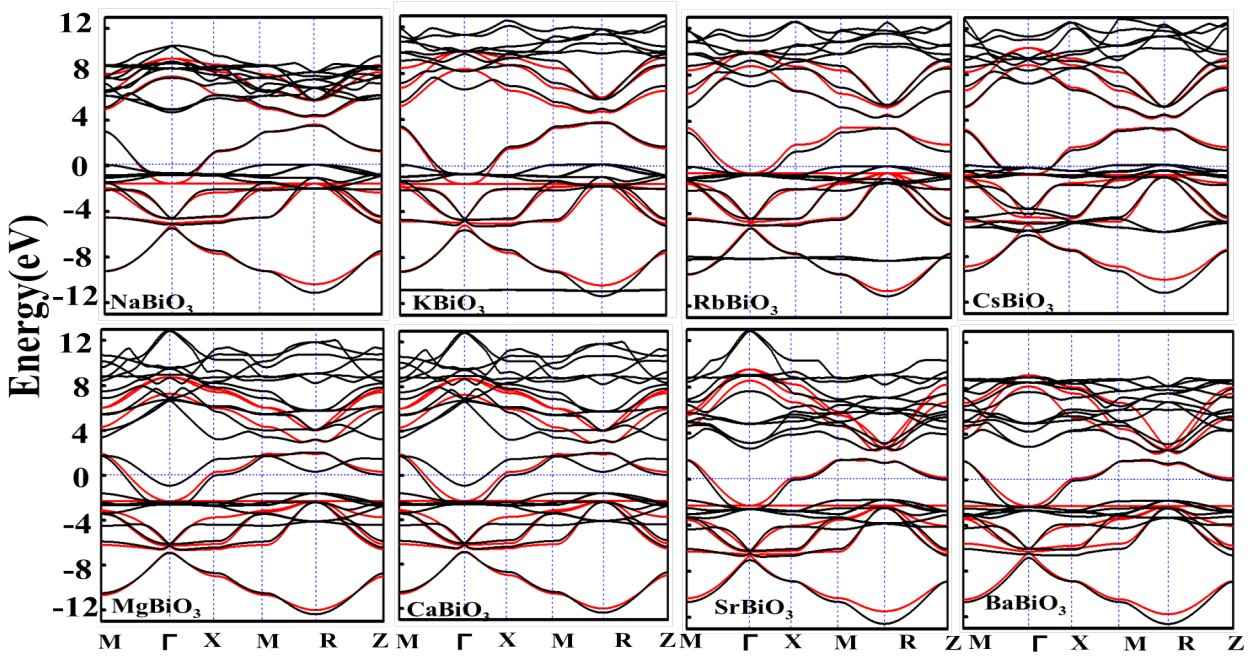

FIG. 10. Same as Fig. 9, except that the SOC is included in the calculations. The SOC either creates a gap at Γ and R or enhances the already existing gaps at these high symmetry points.

TABLE III. Orbital weight factors of different ABiO3 compounds without spin orbit coupling.

	CB orbital weight factors%				VB orbital weight factor %			
	Band index	Bi-s	Bi-p	O-p	Band index	Bi-s	Bi-p	O-p
Na	1	40	0	60	1	100	0	0
	2	0	100	0	2	0	25	75
K	1	41.7	0	58.3	1	0	26.3	76.3
	2	0	100	0	2	0	26.3	76.3
Rb	1	40	0	60	1	100	0	0
	2	0	100	0	2	0	23	77
Cs	1	0	100	0	1	100	0	0
	2	0	100	0	2	0	25.8	74.2
Mg	1	37	0	63	1	100	0	0
	2	0	100	0	2	0	27	73
Ca	1	0	100	0	1	100	0	0
	4	39.8	0	60.2	2	0	24.1	75.9
Ba	1	0	100	0	1	100	0	0
	4	36.6	0	63.4	2	0	25.9	74.1
Sr	1	0	100	0	1	100	0	0
	4	36.7	0	63.3	2	0	25.6	74.4

TABLE IV. Orbital weight factors of different ABiO3 compounds with spin orbit coupling.

	CB orbital weight factors%				VB orbital weight factor %			
	Band index	Bi-s	Bi-p	O-p	Band index	Bi-s	Bi-p	O-p
Na	1	0	100	0	1	0	27	73
	2	40	0	60	2	100	0	0
K	1	0	100	0	1	0	26.5	73.5
	2	41.7	0	58.3	2	100	0	0
Rb	1	0	100	0	1	0	34	66
	2	33.3	0	66.7	2	100	0	0
Cs	1	0	100	0	1	0	31	69
	2	36.2	0	63.8	2	100	0	0
Mg	1	0	100	0	1	0	32.3	67.7
	2	36	0	64	2	100	0	0
Ca	1	0	100	0	1	0	29	71
	4	36.4	0	63.6	2	100	0	0
Ba	1	0	100	0	1	0	28	72
	4	35	0	65	2	100	0	0
Sr	1	0	100	0	1	0	28.6	71.4
	4	36.4	0	63.6	2	100	0	0

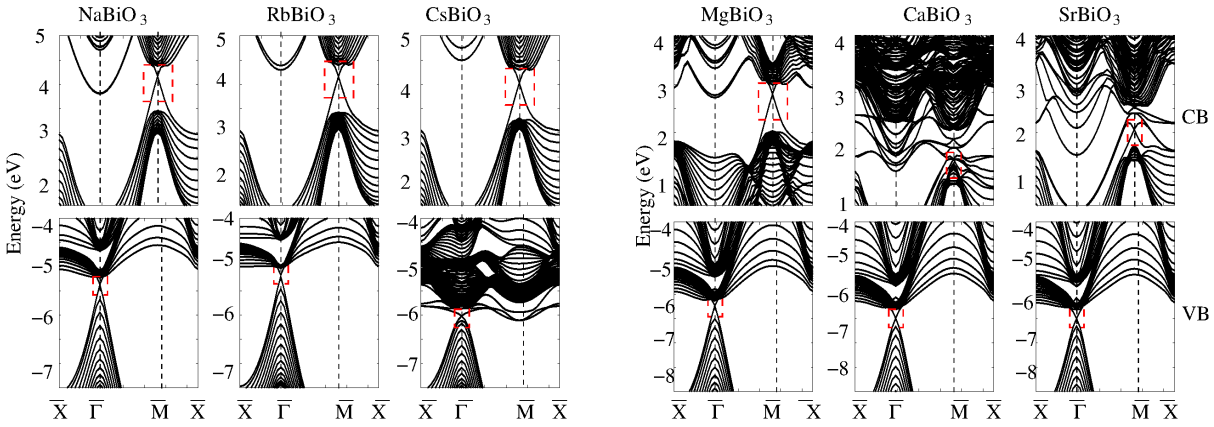

FIG. 11. The Surface band structure for $ABiO_3$ (A=Na, Rb, Cs, Mg, Ca and Sr) along the high symmetry points of the surface Brillouin zone. The first row represents the band structure inside the conduction spectrum, whereas second row is for valence spectrum. Except for A=Na the surface electronic structure is obtained for a 15 unit cell thick $ABiO_3$. For Na 13 unit cell is used. The influence of SOC is considered. The Dirac type surface state appear at two time reversal invariant momenta points for each A is marked with rectangle.

[1] D. Hsieh, Y. Xia, D. Qian, L. Wray, F. Meier, J. H. Dil, J. Osterwalder, L. Patthey, A. V. Fedorov, H. Lin, A. Bansil, D. Grauer, Y. S. Hor, R. J. Cava, and M. Z. Hasan, Phys. Rev. Lett. **103**, 146401 (2009).
[2] L. Fu, C. L. Kane, and E. J. Mele, Phys. Rev. Lett. **98**, 106803 (2007).
[3] M. Z. Hasan and C. L. Kane, Rev. Mod. Phys. **82**, 3045 (2010).
[4] H. Lin, R. S. Markiewicz, L. A. Wray, L. Fu, M. Z. Hasan, and A. Bansil, Phys. Rev. Lett. **105**, 036404 (2010).
[5] D. Xia, Y.and Qian, D. Hsieh, L. Wray, A. Pal, H. Lin, A. Bansil, D. Grauer, Y. S. Hor, R. J. Cava, and M. Z. Hasan, Nat. Phys. **5**, 398 (2012).
[6] T. Sato, K. Segawa, H. Guo, K. Sugawara, S. Souma, T. Takahashi, and Y. Ando, Phys. Rev. Lett. **105**, 136802 (2010).
[7] S. Chadov, X. Qi, J. Kbler, G. H. Fecher, C. Felser, and S. C. Zhang, Nat. Mater **9**, 541 (2010).
[8] J. E. Moore and L. Balents, Phys. Rev. B **75**, 121306 (2007).
[9] X.-L. Qi, T. L. Hughes, and S.-C. Zhang, Phys. Rev. B **78**, 195424 (2008).
[10] D. Xiao, Y. Yao, W. Feng, J. Wen, W. Zhu, X.-Q. Chen, G. M. Stocks, and Z. Zhang, Phys. Rev. Lett. **105**, 096404 (2010).
[11] H. J. Zhang, X. L. Q. C. X. Liu, X. Dai, Z. Fang, and S. C. Zhang, Nat. Phys **5**, 438 (2009).
[12] L. Fu and C. L. Kane, Phys. Rev. B **76**, 045302 (2007).
[13] B. Yan, L. Müchler, X.-L. Qi, S.-C. Zhang, and C. Felser, Phys. Rev. B **85**, 165125 (2012).
[14] H. Zhang, C.-X. Liu, X.-L. Qi, X. Dai, Z. Fang, and S.-C. Zhang, Nat. Phys. **5**, 438 (2009).
[15] M. Yang and W.-M. Liu, Scientific Reports **4**, 5131 (2014).
[16] S. Chadov, X. Qi, J. Kbler, G. H. Fecher, C. Felser, and S. C. Zhang, Nat. Mater **9**, 541 (2010).
[17] B. Yan, M. Jansen, and C. Felser, Nat. Phys. **9**, 709 (2013).
[18] G. Li, B. Yan, R. Thomale, and W. Hanke, Scientific Reports **5**, 10435 (2015).
[19] H. Jin, S. H. Rhim, J. Im, and A. J. Freeman, Scientific Reports **3**, 1651 (2013).
[20] Y. Sun, Q.-Z. Wang, S.-C. Wu, C. Felser, C.-X. Liu, and B. Yan, Phys. Rev. B **93**, 205303 (2016).
[21] Y. Sun, X.-Q. Chen, S. Yunoki, D. Li, and Y. Li, Phys. Rev. Lett. **105**, 216406 (2010).
[22] S.-T. Pi, H. Wang, J. Kim, R. Wu, Y.-K. Wang, and C.-K. Lu, J. Phys. Chem. Lett. **8**, 332 (2017).
[23] D. R. Hamann, Phys. Rev. Lett. **42**, 662 (1979).
[24] J. C. Slater and G. F. Koster, Phys. Rev. **94**, 1498 (1954).
[25] P. Blaha, K. Schwartz, G. Madsen, D. Kvasnicka, and J. Luitz, *WIEN2k, An Augmanted Plane Wave+Local Orbitals Program for Calculating Crystal Properties* (Karlheinz Schwartz, Tech. Universitt Wien, Austria, 2001).
[26] J. P. Perdew, K. Burke, and M. Ernzerhof, Phys. Rev. Lett. **77**, 3865 (1996).
[27] C.-X. Liu, H. Zhang, B. Yan, X.-L. Qi, T. Frauenheim, X. Dai, Z. Fang, and S.-C. Zhang, Phys. Rev. B **81**, 041307 (2010).
[28] X. Luo, M. B. Sullivan, and S. Y. Quek, Phys. Rev. B **86**, 184111 (2012).
[29] G. Vielsack and W. Weber, Phys. Rev. B **54**, 6614 (1996).
[30] Y. Sakamoto, T. Hirahara, H. Miyazaki, S.-i. Kimura, and S. Hasegawa, Phys. Rev. B **81**, 165432 (2010).
[31] K. Park, J. J. Heremans, V. W. Scarola, and D. Minic,

Phys. Rev. Lett. **105**, 186801 (2010).

[32] Q. Liu, C.-X. Liu, C. Xu, X.-L. Qi, and S.-C. Zhang, Phys. Rev. Lett. **102**, 156603 (2009).